Smart Materials and Structures

Improved performance in temperature and speed of TCP artificial Muscles for Soft Wearables Robots by length modification

To cite this article before publication: Alberto Gonzalez *et al* 2023 *Smart Mater. Struct.* in press https://doi.org/10.1088/1361-665X/acded6

IOP Publishing
Journal **XX** (XXXX) XXXXXX

Journal Title
https://doi.org/XXXX/XXXX

Improved performance in temperature and speed of TCP artificial Muscles for Soft Wearables Robots by length modification

Alberto Gonzalez-Vazquez, Lorenzo García, Jeff Kilby.*

Alberto Gonzalez-Vazquez
BioDesign Lab, School of Engineering, Computer and Mathematical Sciences, Auckland University of Technology,1010, Auckland, New Zealand
agonzale@aut.ac.nz

Lorenzo Garcia*
BioDesign Lab, School of Engineering, Computer and Mathematical Sciences, Auckland University of Technology, 1010, Auckland, New Zealand
lorenzo.garcia@aut.ac.nz

Jeff Kilby
BioDesign Lab, School of Engineering, Computer and Mathematical Sciences, Auckland University of Technology,1010, Auckland, New Zealand
Jeffrey.kilby@aut.ac.nz

Abstract

Artificial muscles provide a unique solution for wearable rehabilitation robots (WRRs) because they are compliant, compact, and lightweight. Twisted and coiled polymer actuators (TCPs) are artificial muscles from thermally activated polymer fibres. They present high power density, linearity, stress and strain compared to other artificial muscles. Nevertheless, as TCPs require heat to start, their main barrier for widespread use in WRRs are their slow reaction times and the high temperatures they reach. Previous studies have analysed different parameters, like fibre material, fibre diameter, and various cooling systems, to improve TCP frequency response and working temperature. Nevertheless, the length of the actuator has not been explored as a possible parameter to enhance the actuation performance in this regard.

This work focuses on studying the behaviour of TCPs with different lengths and how the performance in frequency response and temperature can be improved using the length as a primary parameter, as they are critical for wearable robots. First, a characterisation of the TCPs was performed. Then, a method to improve frequency response, based on offsets on long actuators was implemented and validated using a chirp signal. The experimental results show that the mechanical characteristics are similar regardless of the actuator's length. They reached a strain of 10 % with a power of 0.16 W/cm. However, the electrothermal properties changed as the power needed to increase temperature was higher when the actuator was enlarged. Therefore, an improvement in the required temperature was found, able to reduce the temperature with the same frequency response. Regarding the technique to enhance the speed of the actuator, it was possible to increase the frequency by 0.0006 Hz for each mm applied as an offset. Hence, the frequency response for the same displacement was increased linearly as the actuator was elongated.

IOP Publishing Journal Title
Journal **XX** (XXXX) XXXXXX https://doi.org/XXXX/XXXX

Keywords: artificial muscles; twisted and coiled polymer actuators; wearable devices; rehabilitation robots.

Introduction

People with a physical disability caused by conditions like cerebral palsy, stroke, muscular dystrophy, or ageing; face reduced quality of life due to limited mobility and independence (1). The standard rehabilitation therapies used to manage the musculoskeletal system's deterioration and improve or maintain physical ability, include physiotherapy (2). These therapies often involve intensive stretching and strengthening exercises facilitated by the physiotherapist to improve motor skills (3). These interventions are often highly labour-intensive and challenging to perform (4).

During the last decade, wearable rehabilitation robots (WRRs) have gained popularity in rehabilitation (5). WRRs are expected to improve the outcomes of rehabilitation therapies as they allow for mass practice with reduced intervention of the physiotherapists and help people during daily life activities (6). However, most current WRRs use electric motors and rigid links to actuate them and often have heavy and bulky designs that are difficult to wear outside clinical facilities safely (7). Consequently, researchers started to develop soft wearable rehabilitation robots (SWRR) through the use of more compliant elements such as artificial muscles (8) like shape memory alloys (1), dielectric elastomer (9), pneumatic (10), and twisted and coiled polymer actuators (TCPs).

TCPs are artificial muscles fabricated by inserting a twist in precursor polymer fibre while attaching a dead weight at the end until it forms a coil structure, followed by heat treatment (11). To activate the TCPs is necessary to use an external source of heat as they are made of plastic thread. One option is to utilise joule heating by applying an electric current through a conductive heating element embedded into a TCP, such as metallic wires (e.g., Nichrome wires). This method presents the advantage of making the actuators electrically controllable (12, 13). In comparison to other artificial muscles, TCPs stand out due to their high power density (27 W/g), high stress (10 MPa), large strain (21%), and linear behaviour with low hysteresis (14). Nevertheless, they suffer from low frequencies (< 1 Hz) and high temperatures (> 65 °C), all critical aspects for SWRR (14-16).

For SWRR applications, there are biomechanical considerations that need to be fulfilled, like torque/force, range of motion/displacement, and velocity/frequency (17, 18). Due to their advantages, TCPs have gained attention in the SWRR area, as they present high forces and strains. However, they still require improvements in their overall performance as it is still not optimum for the SWRR applications. The main drawbacks are the frequency response and the working temperature.

To overcome these drawbacks, researchers have investigated how different TCPs parameters and techniques impact the actuators' frequency response and working temperature to be used on SWRRs. Hiraoka et al. (19) used hard linear low-density polyethene (LLDPE) fibres to improve the operating temperature. Haines et al. (20) demonstrated that the response time depends on the fibre diameter. Yip et al. (21) used a closed-loop control strategy to improve the speed of the fibres during the heating phase. Edmonds et al. (22) showed how an active cooling system can increase the maximum frequency where the TCPs can work.

Even if length is one of the primary parameters to consider when designing an application, there is no literature exploring the use of length to improve the response time and temperature of the TCPs. Therefore, this article explores how different lengths impact the actuator's temperature and response time behaviour. Furthermore, a new methodology is presented to improve the TCP frequency response based on the actuator's length without using external cooling systems.

This work is divided into four parts: the first one, Section 2, aims to investigate the length impact on the TCPs behaviour by using TCPs of three different lengths (75, 180 and 295 mm) in isotonic contraction (i.e., the muscle contract generating a displacement). The second part, Section 3, implements a methodology to improve the frequency response and manage the operational temperature base on the length of the actuator and a PID displacement control. Then, Section 4 discusses the advantages of longer fibres in wearables rehabilitation robots. Finally, a conclusion is presented in section 5.

Actuator Characterisation

An isotonic contraction test was applied to the TCPs to characterise the actuators and understand their properties in force, strain, response time and temperature, as they are the main requirements for SWRR.

2.1 Materials and Methods

The TCP actuators to be analysed were fabricated similarly to the process described by Chossat et al. (23). 1.25 m Nylon fishing line was used as the precursor fibre (Trilene Big Game fishing line 50 lb) with a diameter of 700 µm. The nylon fibres

were twisted and coiled along with a 36 AWG (127 μm) Nickel-Chromium 80 (NiCr) wire (Fogslord). One side of the nylon fibre was fixed at the end of the output shaft of a NEMA17 (T-Trees Technology) motor. The other end is on a slider weighing 800 g (≈20 MPa). The NiCr wire was also suspended from the motor shaft but only straightened using a small weight of 1.6 g (≈1.2 MPa) and was left free to untwist. The fibres were twisted and coiled at a slow speed of 250 rpm (24). The embedded NiCr wire generated joule heating for the annealing phase. The annealing process involves applying five consecutive five-minute-long periods with an annealing current of 240 mA each. Between every period, a cooling phase of 1 minute was used.

After this process, TCPs with an average length of 330 mm were obtained (Fig. 1a). They were manually trimmed into three sizes of approximately one-quarter, two-quarters, and three-quarters of the initial measurement. They resulted in actuators with a length of 75 mm, 165 mm, and 250 mm. Then the outcoming actuators were clamped with insulated male spade electric terminals, reducing the functional area by 10 mm as each electrical terminal required 5 mm to be crimped (Fig. 1b). The final active lengths of the TCPs were 65 mm, 155 mm and 240 mm with resistance values of 25 Ω, 59 Ω and 92 Ω respectively, meaning that all of them present a resistivity $\rho \approx 0.38$ Ω/mm. The relation between length and resistance can be described with a linear approximation:

$$R = 0.38281 \times L - 0.0305 \quad (1)$$

where R is the resistance (in ohms), and L is the actuator's length (in mm).

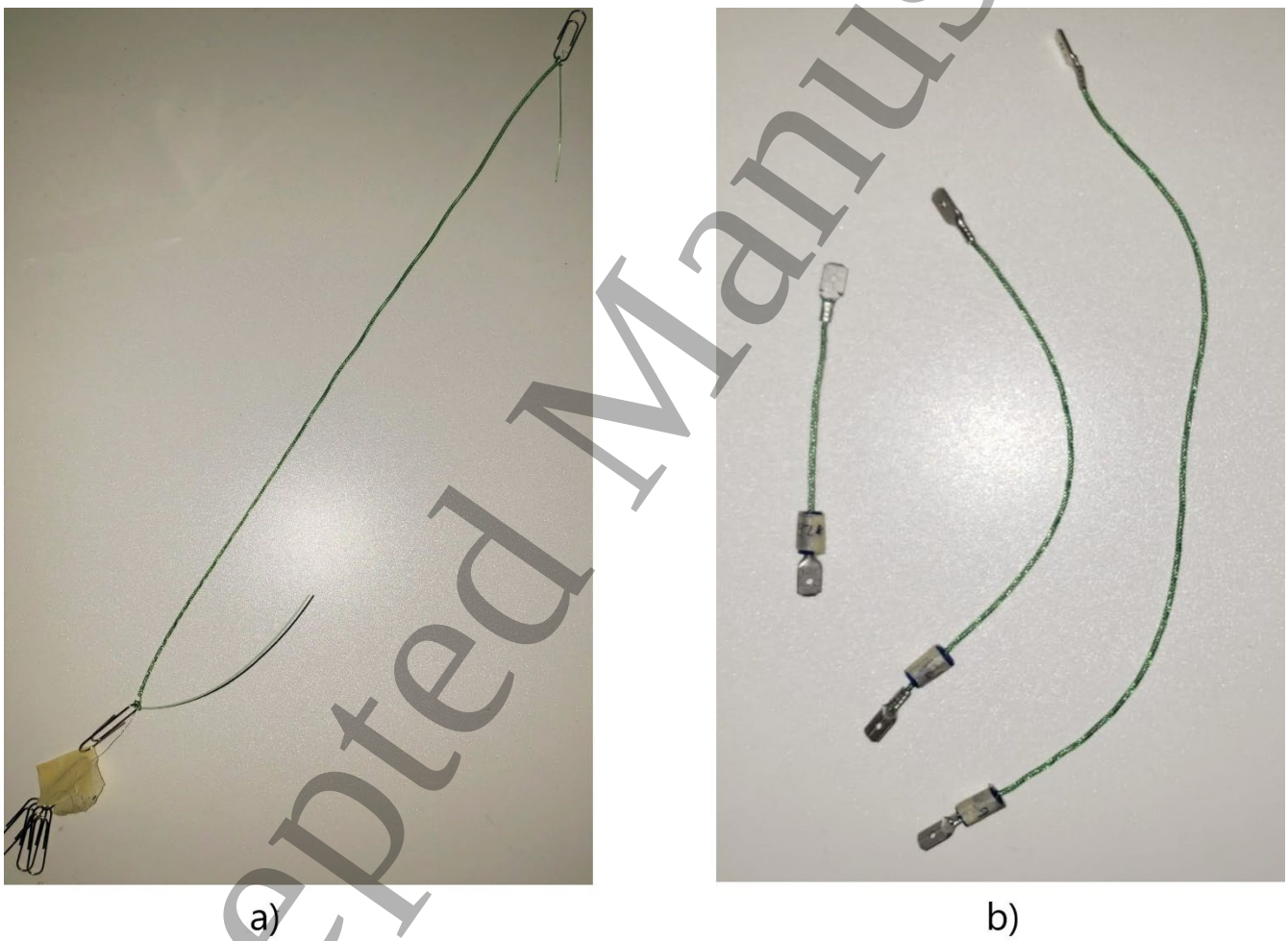

Figure 1. TCP actuators, a) Initial actuator, b) actuators of different sizes with spade electric terminals.

Three TCP actuators of each size were manufactured, following the mentioned method. All the samples fabricated for the study were tested using a custom-made experimental test bench. The experimental setup consists of a displacement sensor (Sick

Optex 0d80 15p850) connected to a current sensor (Texas Instruments INA269), an Arduino NANO connected to the computer, and a transistor (Vishay Siliconix IRF540) to control the voltage coming from the power supply. The actuator was hanging above the sensor, weighing 700 g. Furthermore, the temperature and the power to activate the TCP were measured using an NTC thermistor (5K3A1, TE Connectivity) and an extra current sensor (Texas Instruments INA269).

A square signal of 150 s on and 150 s off was applied to obtain the strain and power relation. The 150 s was chosen to give enough time to the system to reach a stable condition. The experiment was repeated for different current levels ranging from 160 mA to 220 mA with increments of 20 mA. After applying the load (700 g), the actuator's length was 75 mm, 180 mm and 295 mm. The loaded lengths were the ones used in the results section. Throughout the trial, the TCA temperatures, power consumed, and the weight distance from the sensor were logged into a computer using an Arduino NANO with a sampling time of 50 ms. This test was performed for every actuator of different sizes.

2.2 Results

After performing all of the trials for each different size, the resulting power, displacement, and temperature values were obtained (Fig. 2). The power consumption was derived from the applied current and the resistance values of the different actuators. When full power was applied to the actuators (1.2 W, 2.8 W and 4.5 W, respectively), the maximum achieved displacements were 7.12 mm, 17.1 mm, and 28.9 mm for the 75 mm, 180 mm, and 295 mm, respectively. The maximum strain of all the TCP of different sizes was ≈ 10 % of the initial length. Regarding the temperature (Fig. 2g-i), the maximum average temperatures obtained were 81.26 °C, 80.36 °C, and 76.83 °C for the 75 mm, 180 mm, and 295 mm TCP actuators, respectively.

Other interesting information that can be obtained from the data is the rise (τ_r) and fall (τ_f) response times of the actuators. This is the average time the actuator takes to reach 63% of a steady-state value given a step input. For the 75 mm actuators, $\tau_r = 17.98\ s$ and $\tau_f = 14.51\ s$. In the case of the 180 mm actuators, the τ_r and τ_f were 22.59 s and 16.10 s, respectively. Finally, for the 295 mm actuators, the τ_r and τ_f were 23.58 s and 16.49 s.

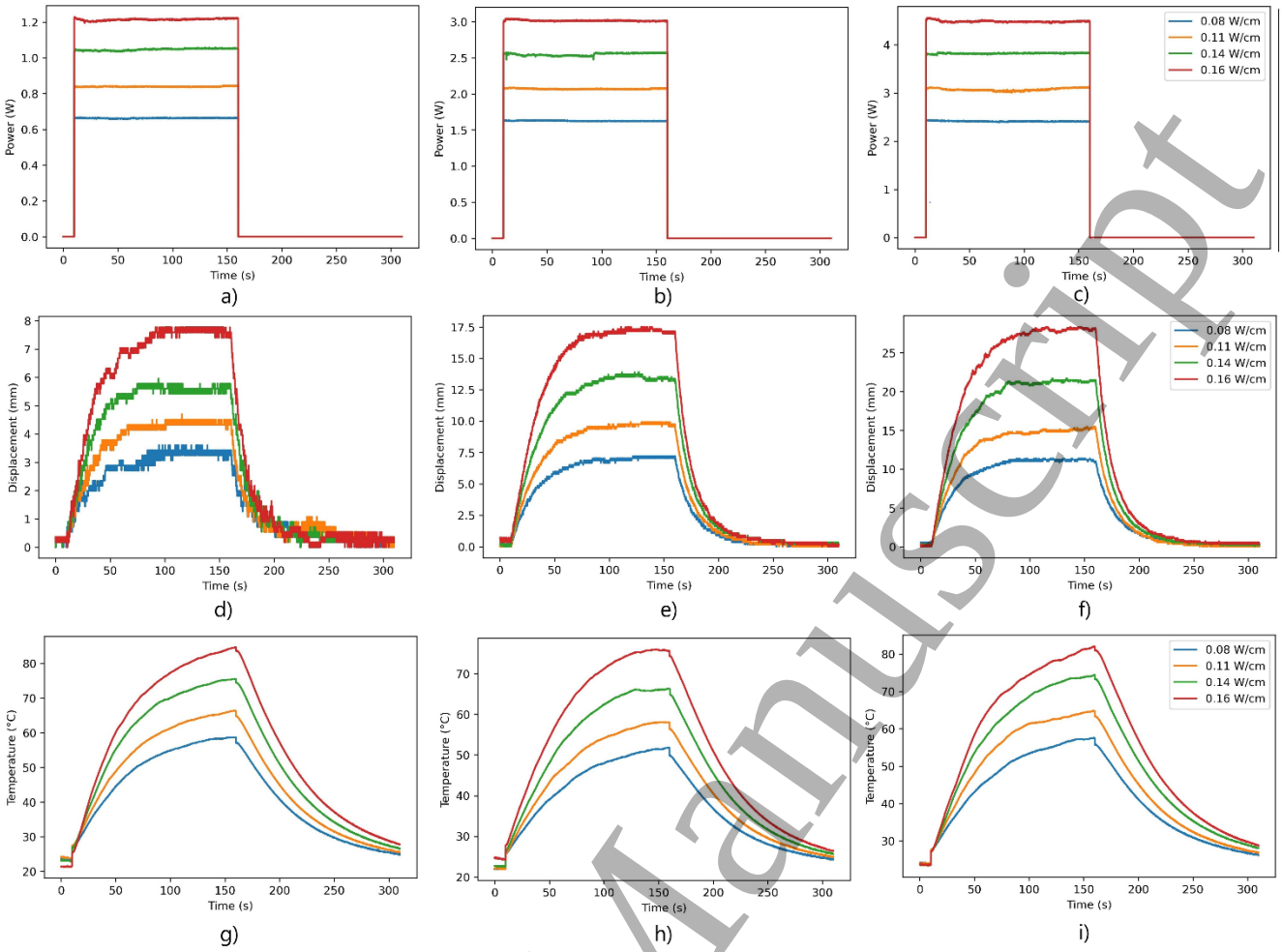

Figure 2 Power consumed by the actuators during the isotonic contraction tests a) 75 mm, b) 180 mm, c) 295 mm. Resultant contraction from the actuator during the isotonic contraction test d) 75 mm, e) 180 mm, f) 295 mm. Reached temperatures from the actuator during the isotonic contraction test g) 75 mm, h) 180 mm, i) 295 mm.

The stroke and power levels were calculated for each set of actuators. Then, a linear regression was applied to the mean values of each set of actuators to determine a linear model. In Fig. 3a, the linear relation between the applied power in W and the generated stroke can be seen. From this relation, it is possible to observe that, independently of the length of the actuator, the applied power will generate the same amount of stroke. This relation can be represented as (R^2=0.9708):

$$D = 6.1033 \times P - 1.6426 \quad (2)$$

where D is the generated stroke in mm, and P is the required power in watts.

Furthermore, the idea remains that the relationship between the stroke and the applied power is independent of the actuator length. The TCP length normalised the stroke and the power during the experiments (Fig. 3b), and the following linear relation was obtained (R^2 = 0.9821):

$$S = 75.2979 \times NP - 2.6920 \quad (3)$$

In this case, S is the strain of the actuator, and NP is the normalised power (W/cm). The strain of the system is the relation between the initial length (L) of the actuator and the generated stroke (ΔL) when activated, expressed in % as follows:

$$S = \frac{\Delta L}{L} \times 100 \quad (4)$$

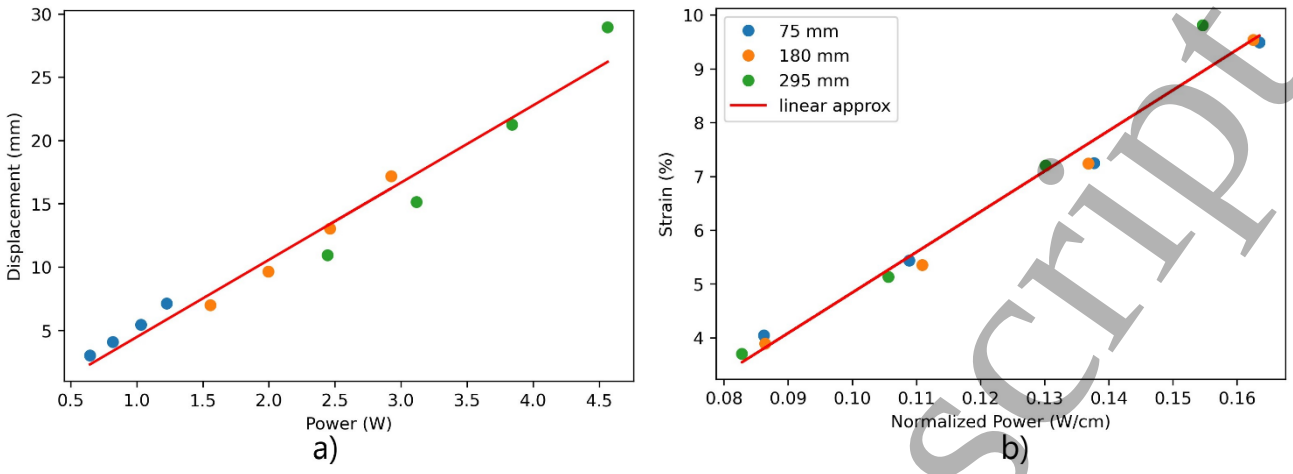

Figure 3 Maximum displacement relation with respect to power, with overlaid linear regression, b) normalised to TCP length relation.

Regarding the temperature, a linear trend was found between the temperature and the applied normalised power (R^2 = 0.9624):

$$T = 326.9759 \times NP + 27.0464 \quad (5)$$

Where T is the temperature in °C and NP is the normalised power. Finally, a linear relation was found between temperature and strain (R^2 = 0.9296):

$$S = 0.2204 \times T - 8.2573 \quad (6)$$

With the observed relation (equation 3), it is possible to witness that independently of any unit of length, the strain stay the same due to the asymmetric thermal expansion of polymer monofilaments (11). Nevertheless, when it comes to the thermal properties, they will change with the length of the actuator (25). The central values on the electrothermal relation (equation 7) are dependent on the length (thermal resistance (R_{th}) and thermal capacitance (C_{th})) (Fig. 4a). The dependency on length could be seen in equation 8 and equation 9 as it forms part of the surface area and volume; respectively.

$$C_{th}\frac{dT(t)}{dt} = P(t) - \frac{(T_{tcp}(t) - T_{\infty})}{R_{th}} \quad (7)$$

Where C_{th} is the thermal capacitance, P is the applied power, R_{th} is the thermal resistance, T_{tcp} is the surface temperature of the TCP and T_{∞} the ambient temperature.

$$R_{th} = \frac{1}{A_{tcp}\, x\, (h + \varepsilon_{tcp} \times \sigma \times (T_{tcp} + T_{\infty}) \times (T_{tcp}^2 + T_{\infty}^2))} \quad (8)$$

R_{th} can be calculated using the surface area A_{tca}, the thermal convection coefficient h, the emissivity ε_{tcp}, the Stefan Boltzmann's constant σ, and the temperatures generated by the TCP T_{tcp} and the environmental temperature T_{∞}. Moreover A_{tca} can be calculated with:

$$A_{tcp} = 2\pi rL + 2\pi r^2 \quad (9)$$

Being the r the radius of the TCP cross sectional area and the actuator length L .

$C_{th} = \rho\, x\, c\, xv$	(9)

Finally, C_{th} is obtained multiplying the ρ density, the specific heat capacity c and the volume of the sample v.

It is possible to see the advantages of implementing long actuators into WRR. It is feasible to obtain the same stroke using the same amount of power from a more extended actuator rather than a small actuator's full stroke range and reduce the generated temperature from the TCP actuator (Fig. 4 b-d) without increasing the time. The main disadvantage of the actuator's increases in length, is the R_{th} decrease as the surface area increase (equation 8). The change in R_{th} will cause an increase in power consumption to generate the same temperature (equation 7). Nevertheless, the response time will remain similar:

$\tau = C_{th}\, x\, R_{th}$	(10)

where is possible to notice from equation 8 and equation 9 that the increased and decreased values of C_{th} and R_{th} will change in the same linear manner with the length of the actuator.

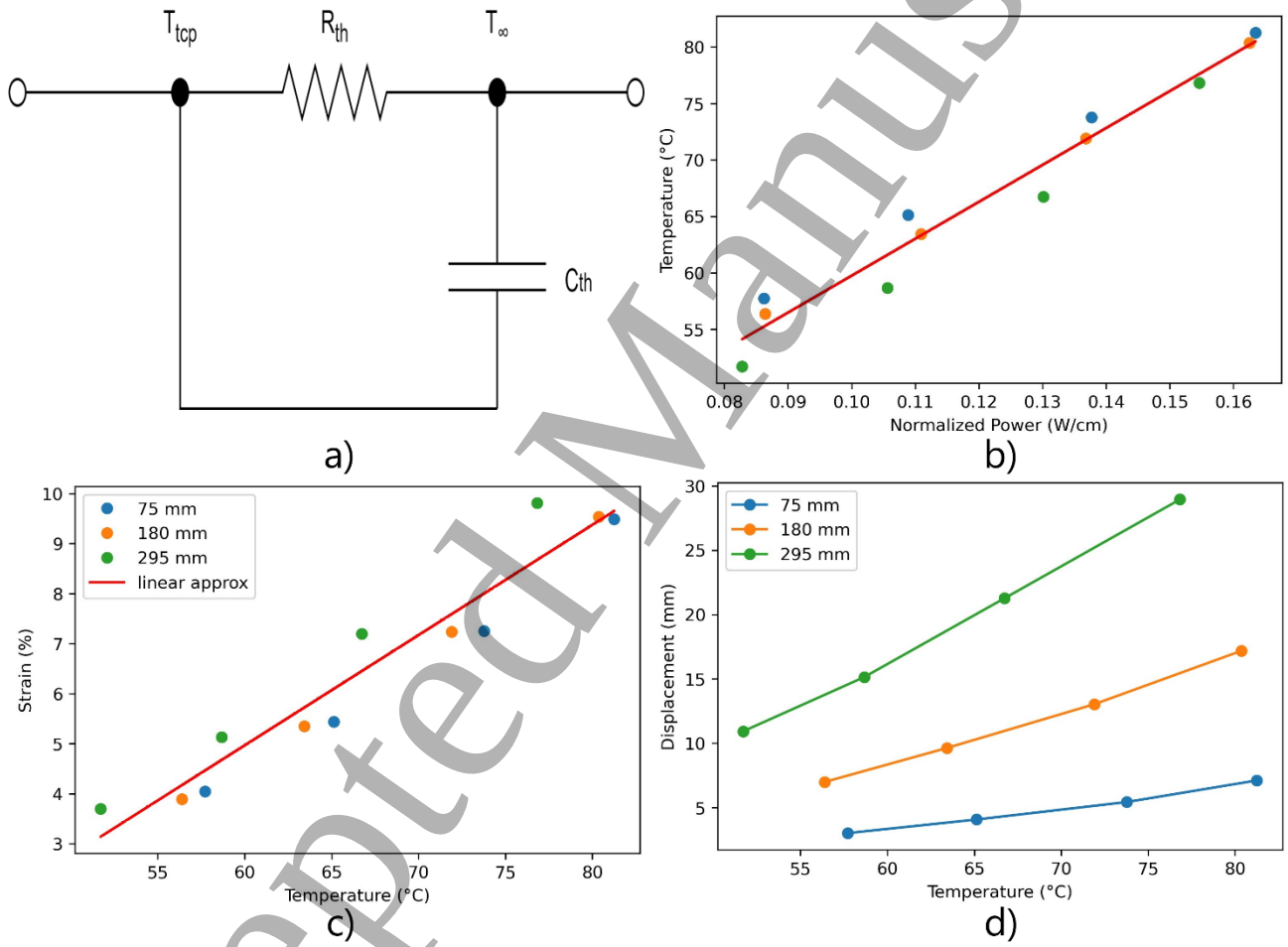

Figure. 4 a) Simplified thermal model of the TCP, consisting of the thermal capacitance C_{th}, the thermal resistance R_{th}, the TCP surface temperature T_{tcp} and the ambient temperature T_{∞}. Temperature relations during the isotonic contraction test. b) Temperature against the normalised power, and c) strain versus temperature. d) Generated displacement with the three different lengths against the temperature.

Displacement Control Implementation

In the previous section, the characterisation of the TCP actuators was performed. Furthermore, the advantage of a reduction in temperature using longer actuators was found. However, one of the main disadvantages of TCPs is the low frequencies at which they can work (<1 Hz). A strategy to increase the response time could be to briefly apply a pulsed signal with high power peaks (12, 26). However, the continuation of a high-power pulse will produce an overheating of the actuator, causing it to break or burn out (27). Hence, a control strategy should be applied to avoid overheating the actuator and work under safety actuation ranges. However, this strategy can only be used during the rising time but not during the falling time, as TCPs are unidirectionally actuated. A popular approach to reducing the response time during the falling time is to implement a cooling system, decreasing the overall response time, with the constraint of requiring external equipment like pumps or fans (21, 22).

This section investigates a method to improve the actuation speed but using long actuators. From the isotonic test in the previous section, it could be seen that length impacts the actuation temperature, as it is possible to obtain a more significant displacement with a lower temperature. Furthermore, Cho et al. (28) show that the falling time in the temperature of the TCPs depends on how different the final temperature is from the starting temperature. Moreover, Tang et al. (29) proposed to constrain the range of the activation to improve the speed of a crawling robot. Considering the previous concepts, a method combining both approaches is presented and analysed on how the actuator length could benefit from them and increase the frequency without needing an external cooling system. The technique consists of actuating a specific displacement using different displacement offsets on the actuators. As the actuator lengthens is possible to add more offsets, which will change the actuation range in temperatures, increasing the actuation speed as the cooling time is reduced.

3.1 Materials and Methods

After characterising, in section 2, the strain production of the actuator in an open-loop system, a closed-loop control scheme to operate the displacement output of the actuator is provided. Two different experiments were performed to test the response of the controlled system. First, a step signal was used to analyse the response time while heating, and later a chirp signal was used to analyse the system's frequency response on the proposed control method based on the actuator length.

The test bench was the same as in the characterisation experiments (section 2), with two differences. The sensor reading the current across the TCP was removed due to the higher power values needed to activate the actuator when the PID controller is on. Instead of using the MOSFET as a digital on-off switch, a power pulse width modulation (PWM) strategy was implemented (100 ms cycle time). It allows the usage of high-power signals controlled by the microcontroller. The power was constrained to 0.86 W/cm, equal to 6.5 W, 16.4 W, and 25.5 W for the 75 mm, 190 mm and 295 mm, respectively. The maximum applied power was chosen due to limitations with the power supply at full power.

3.2 System Identification

The controller was constructed based on the stroke characterisation experiment results, which generated a time-domain relationship between stroke output and the input power. The input signal was the maximum applied power for each actuator size, and the output signal was the generated displacement. Later, the curves' pairs were input into the System Identification Toolbox in MATLAB, which derived the power–displacement transfer functions G_{PD} (s) for each actuator length (Table 1). The proposed model by Yip et al. (21) was used as the initial guess to find the order of the transfer function. In this work, the model was divided into a temperature-force relation, a power-force relation, and a force-movement relation.

First, a temperature-force relation was modelled as a spring and damper model with the addition of a linear temperature-dependent term:

$$f(t) = k(x - x_0) + b\dot{x} + c(T(t) - T_0) \tag{11}$$

Where f is the force of the system, k is the spring constant, b is the damping coefficient, c is the thermal constant, x is the position, x_0 is the initial position and $\dot{x}$ is the speed.

When the wires are held in isometric tension, the force can be modelled by:

$$f(t) = c(T(t) - T_0) \tag{12}$$

To obtain the power-force relation, equation 12 is combined with the thermoelectric model of the actuators (equation 7):

$$\frac{F(s)}{P(s)} = \frac{c}{C_{th}s + \frac{1}{R_{th}}} \tag{13}$$

Then to obtain the force-displacement relation can be modelled as a second-order mass-spring-damper system:

$$f = m\frac{d^2x}{dt^2} + b\frac{dx}{dt} + k(x - x_0) \quad (14)$$

That will result in the following transfer function:

$$\frac{X(s)}{F(s)} = \frac{1}{ms^2 + bs + k} \quad (15)$$

Finally, combining equation 13 and equation 15, a third-order system of the following form is obtained:

$$\frac{X(s)}{P(s)} = \frac{A}{Bs^3 + Cs^2 + Ds + E} \quad (16)$$

A, B, C, D, and E are values derived from the model constants.

The initial estimation of the system was a third-order transfer function with no zeros. However, it was noticed that adding a zero increased the system's accuracy (Table 1). Hence the used models were those with one zero.

Table 1. Frequency domain transfer functions for the power–stroke relationships $G_{PD}(s)$ with one or non-zero for each actuator size

Actuator size (mm)	G_{PD} (no zero)	Accuracy	G_{PD} (1 zero)	Accuracy
75	$\frac{0.2815}{s^3 + 4.295\,s^2 + 1.232\,s + 0.4748}$	94.8%	$\frac{5.947\,s + 3.119}{s^3 + 55.48\,s^2 + 13.73\,s + 0.5228}$	96.47%
180	$\frac{0.0003572}{s^3 + 0.162\,s^2 + 0.0061\,s + 5.77e^{-5}}$	93.82%	$\frac{1.326\,s + 0.1758}{s^3 + 7.25\,s^2 + 0.8503\,s + 0.02774}$	98.98%
295	$\frac{0.0003575}{s^3 + 0.1514\,s^2 + 0.00643\,s + 5.55e^{-5}}$	97.85%	$\frac{14.53\,s + 2.132}{s^3 + 89.27\,s^2 + 11.24\,s + 0.3366}$	98.93%

3.3 Control strategy

When using the transfer functions, a proportional-integral-derivative (PID) controller was tuned using the Control system toolbox in MATLAB. Then the closed loop with the PID controller system was simulated in MATLAB/Simulink. In particular, special care was taken to minimise the overshoot, settling error of the controller, and the necessary power to activate the system, as errors of that nature would result in an incorrect application of force to the user, which could cause harm.

Applying the maximum power, the speed to achieve the highest contraction (10 % of the initial length) was 7.5 s. However, the values for a reaction time of 1 s equivalent to a frequency of 1 Hz were also investigated and applied in the chirp test. As most activities of daily life (ADLs) frequencies are around 1 Hz (30, 31). According to Table 2, the PID values are similar for all the different lengths. The values obtained for the 295 mm model were used, as this model was the best of the 3 cases obtaining accuracies over 83% when fitting to the data.

Table 2. PID controller values

Actuator length (mm)	Speed (s)	KP	KI	KD
75	7.5	1.394	0.08267	0
180	7.5	1.309	0.07955	0
295	7.5	1.484	0.08365	0

295	1	12.05	4.408	0

After the closed-loop controller was tuned, it was implemented on an Arduino NANO microcontroller. Two different tests were performed. First, a step input test was applied to determine their performance in controlling the actuator, and then a chirp test was used to test the bandwidth of the actuator.

3.4 Results

3.4.1 Step Response

The step response was applied to the full stroke (a strain of 10 %). Fig. 5a shows the position reference and the output when a step signal was applied for the different actuator sizes. It can be observed that the output follows the reference, but the system presents an underdamped response. The time from 0 to 10 % of the initial length was less than 10 seconds. Contraction time can be minimised by changing the controller gains, but an aggressive control signal will increase the peak power required to produce the change.

Nevertheless, the falling time was the same as the open-loop system and depended on the convective air to cool down the system. From Fig. 5c, it is possible to notice the difference between the required power to make a fast movement and the power to maintain a steady state. In the case of the steady-state power, once the actuator reaches a steady-state, the consumed power is similar to the power required on the open-loop system (approx. 1.2 W, 2.13 W and 3.1 W for the 75 mm, 180 mm and 295 mm, respectively). The consumed power was calculated as a function of the percentage of the duty cycle on the PWM. Fig. 5d shows the percentage of the PWM duty cycle, and it can be noticed that the PWM values are similar for all the sizes. Finally, Fig. 5b shows the reached temperatures during the experiments. They were comparable to those obtained during the open-loop experiments, with the difference of a faster temperature increase at the beginning due to the higher applied energy. Interestingly, in any case, the temperature surpassed 70°C-80°C, which were the maximum temperatures before the actuator failed.

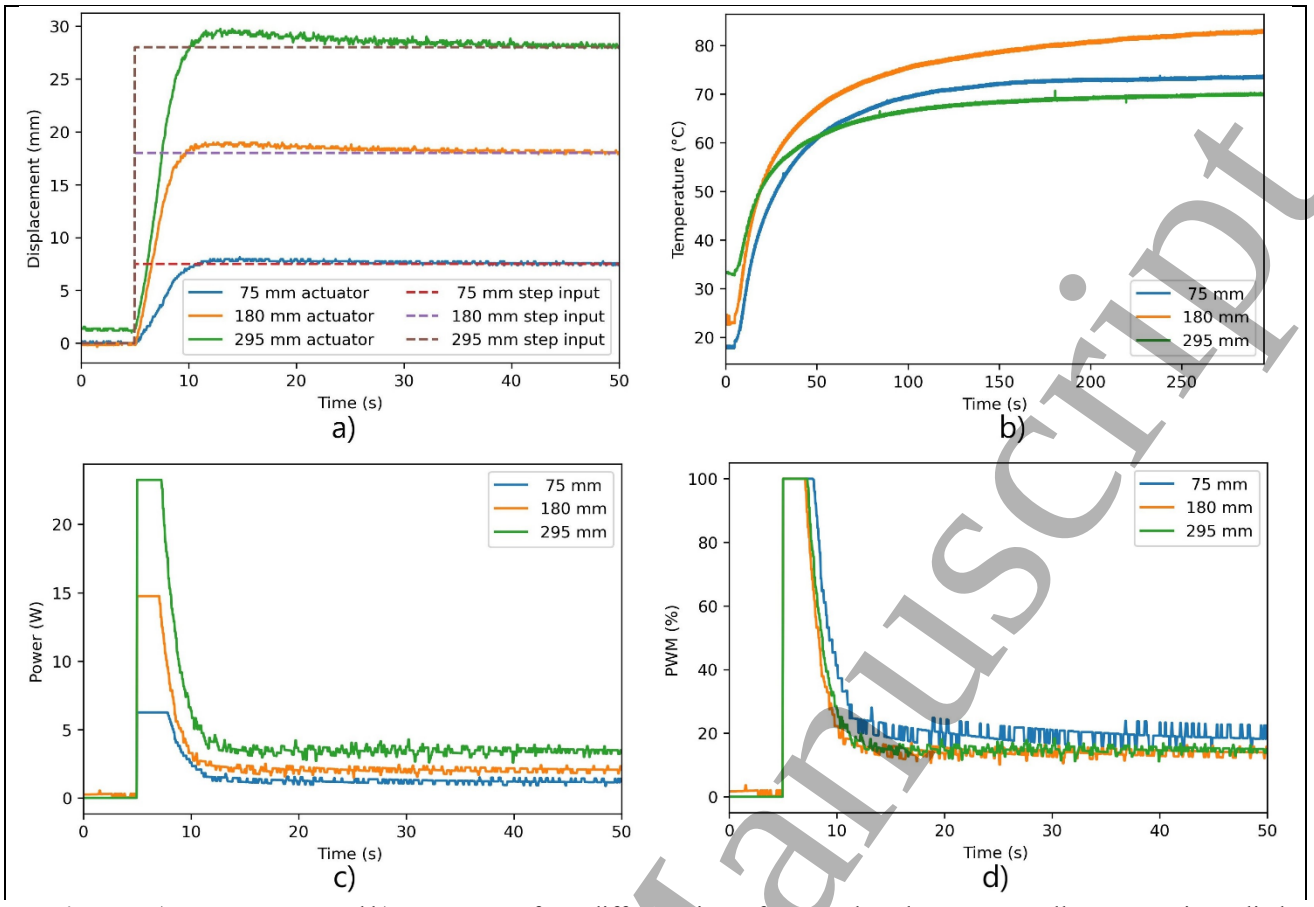

Figure 5 a) Step response and b) temperature from different sizes of TCPs when the PID controller strategy is applied. PWM control signal expressed c) in consumed power and d) in % of the PWM.

3.4.2 Chirp response

The benchmarking for the actuator speed using the proposed variable length method was performed by applying a linear chirp signal (32). It consists of a sinusoidal sweep signal that varies its frequency over time, which can be expressed as follow:

$$chirp(t) = \mathrm{A}\sin\left[2\pi\left(\frac{c}{2}t^2 + f_0 t\right)\right] \quad (17)$$

Were f_0 is the final frequency, A is the amplitude of the sinewave, and c is the chirp rate, described by:

$$c = \frac{f_e - f_0}{T} \quad (18)$$

where f_e is the final frequency, and T is the time it takes to sweep from f_0 to f_e.

The sinewave amplitude was 6 mm for testing, making the base displacement 1 mm - 7 mm. This was chosen to use the whole stroke of the 75 mm actuator. From here, offsets of 60 mm were applied to the longer actuators. Hence, in the case of the 180 mm, experiments with a maximum displacement of 7, 13 and 19 mm were performed. Moreover, with the 290 mm, a maximum displacement of 25 mm was added.

The initial chirp frequency was 0.01 Hz. This frequency was chosen as it is lower than 0.05 Hz, which is the inverse of the response time of the actuator (τ_f = 23.58 s). Furthermore, the final frequency is equal to 0.1 Hz, near the maximum frequency of the controller speed of 7.5 seconds (0.133 Hz). In the case of the final frequency, it was chosen to be lower than the inverse of the maximum rate with the controller, as the controller only works in the contraction direction, making it slow when cooling down. The maximum working frequency for each TCP was established when the actuator lost -3dB in amplitude (when the active actuator range was reduced by half) in the frequency analysis of the output signal.

As with the previous experiments, the behaviour of the lower range in the 180 mm and 290 mm actuators was similar to using a 75 mm (except the maximum temperature), and the same applies to the 180 mm to with the 290 mm, meaning that the linear behaviour of different lengths is still valid. Due to these similarities, Fig. 6 presents only the result of the 290 mm TCP at various levels.

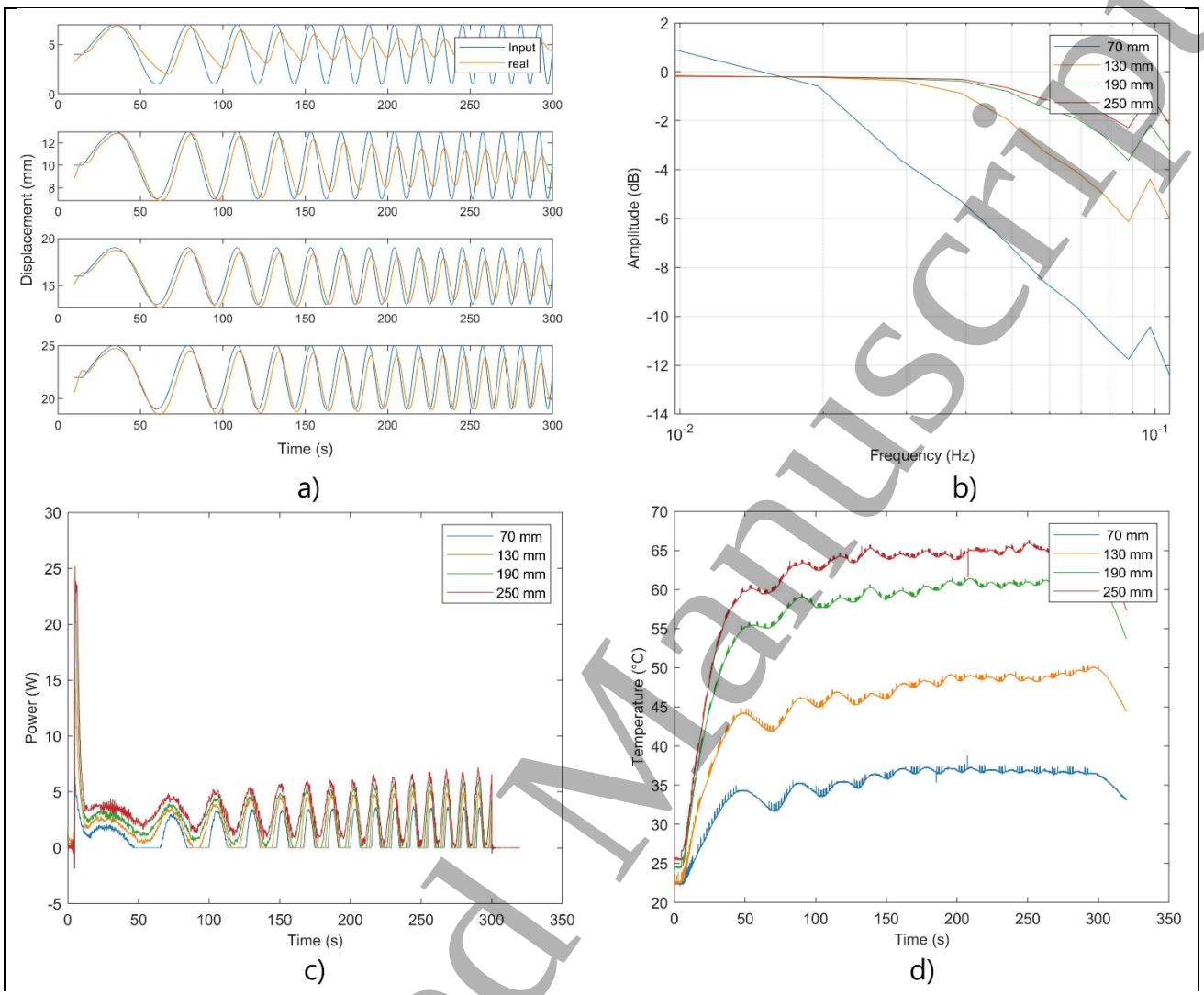

Figure. 6 a) Position response with chirp signal reference (0.01-0.1 Hz) to different offsets on the 295 mm TCP with a 7.5 s response time PID controller. b) Magnitude Bode plot for the 295 mm with different offsets. C) Power consumption corresponds to the chirp test response (0.01-0.1 Hz). d) Reached temperatures during the chirp test.

After analysing the data of the 190 mm TCP, there was a slight difference between the 120 and 180 mm offset, and neither reached the -3 dB in amplitude (Fig. 6a-b). Furthermore, during the test, the maximum power was only applied at the beginning of the test to reach the offset. After that, the used power was less than half of the maximum power (Fig. 6c). Hence, a new chirp was used, but this time with a maximum frequency of 1 Hz, PID values were changed to those that allowed the actuator for 1 s reaction times (Table 2). In the case of the temperature, as the speed increases, it reaches temperatures as if a step signal were applied. This is because the system can't respond to those frequencies and starts behaving like a DC voltage signal (Fig. 6d).

Table 3 shows the maximum temperature reached during the test, the frequency at -3dB, and the peak power consumption at this frequency for each actuator and offset.

Table 3. Maximum values of the 1 Hz Chirp Test

Actuator (offset)	Maximum temperature (°C)	Frequency at -3dB (Hz)	Power at -3dB (W)

75 mm	72.74	0.051	4.0
180 mm	45.5	0.046	4.16
180 mm (60 mm)	60.35	0.09	7.63
180 mm (120 mm)	71.4	0.127	10.15
295 mm	40.03	0.043	4.27
295 mm (60 mm)	52.17	0.082	7.78
295 mm (120 mm)	63.23	0.11	10.19
295 mm (180 mm)	71.07	0.15	13.64

After increasing the chirp frequency and the PID controller, the difference between 120 and 180 mm offset increases. Both reach the mark of -3dB in amplitude at different frequencies, 0.11 and 0.15 Hz, respectively (Fig. 7a-b). It is possible to appreciate how the response time of the actuator change as the offset is increased in both time (Fig. 7a) and frequency domains (Fig. 7b). In this case, as the speed increases, the maximum power starts to be used during the activation time to achieve the actuation at the high frequencies (1 Hz). Nevertheless, during relaxation times, the cooling process is slow. This slow cooling process is what sets the frequency. The temperature was not pictured for the 1 s PID as the temperature tends to be a constant similar to that achieved during the step test.

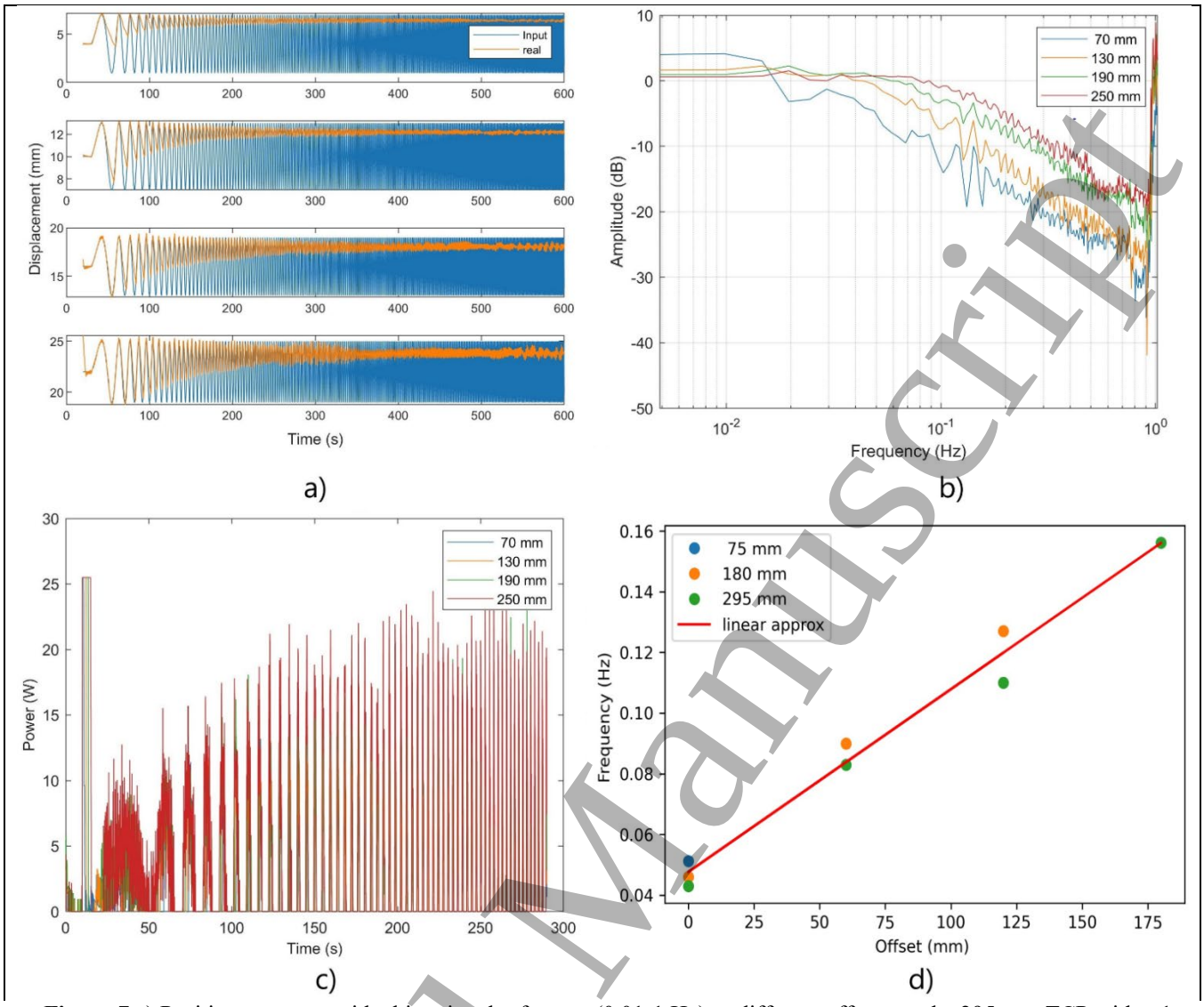

Figure 7 a) Position response with chirp signal reference (0.01-1 Hz) to different offsets on the 295 mm TCP with a 1 s response time PID controller. b) Magnitude Bode plot for the 295 mm with different offsets. c) Power consumption for the 295 mm with different offsets (0.01-0.5 Hz). d) Linear relationship between offset increment and frequency increment.

When the reached frequencies (F) are compared to the given offset a linear relation was found ($R^2 = 0.9809$):

$$F = 0.0006 \times Offset + 0.0477 \quad (16)$$

For every mm increased as an offset a gain of 0.0006 Hz is obtained. In the proposed example, the initial frequency of the 6 mm displacement was 0.051 Hz, and it improved to 0.15 Hz with the 295 mm actuator (approximately three times faster). The change in the frequency is due to the displacement range used. The relation is independently of the length of the actuator, it can be seen the trend of the 180 mm and 295 mm actuator are similar for the first two offsets. Furthermore, the maximum temperature was almost the same for the faster test on the 295 mm than in the case of the 75 mm, providing an advantage as it is possible to reduce the temperature with the same or better performance in speed. However, the consumed power will increase (Fig. 7c) as higher frequencies require more significant offsets.

Discussion

This work presents the properties of long TCP actuators to increase the bandwidth and reduce the working temperature to explore their use on WRR.

From the result of the characterisation test, the length does not affect the maximum stroke that an actuator can generate, as all the different sizes presented a strain of ≈ 10% of the initial length. Furthermore, the mechanical properties are maintained, and a linear relationship was found between the applied power and the achieved stroke.

Another advantage is the temperature reduction to generate a particular stroke as the actuator length increases. This advantage is a crucial design feature for SWRR using thermally activated actuators, as the temperature for the pain threshold of humans is 44 °C at the dermal/epidermal interface of the skin (16). Meanwhile, if the actuator is activated at its full range, it can reach a temperature above 70° C (Fig. 4b).

For example, in the case of a wrist SWRR, which requires a range of motion (ROM) of 40° extension and 38° flexion during activities of daily life (ADLs), a stroke of ≈ 23 mm is needed (22). From the used actuators, the most similar to get this length with the maximum stroke will be 180 mm; at its maximum stroke ≈ 18 mm, the temperature is ≈ 82°. In contrast, if the 295 mm actuator is used to obtain the same displacement, the temperature will be ≈ 62°. And it can be reduced more if a longer actuator were to be used. Furthermore, space should not be a constraint. Like shape memory alloys (33), TCP actuators could be wrapped around pulleys (16, 34) to utilise longer muscle lengths allowing larger strokes.

Regarding the speed of the actuators, during open-loop activation, there is no difference between the different lengths of actuators as the time response is similar, independently of the length. In the case of the fabricated actuators, it was around 20 s. Nevertheless, reaching high contraction speeds independently of the length is possible with a correct closed-loop control strategy and high-power values. Furthermore, as the electromechanical model is similar for all the lengths, using the same PID controller is possible.

As noticed from previous research (21, 22), the problem with the TCP actuators is the cooling time to recover the initial length, which is found during the isotonic contraction tests. The typical method to improve the speed is to reduce the TCP diameter with the disadvantage of reducing the force or using a cooling system that will increase the system's complexity. In this work, a different strategy is proposed for single TCP actuators. The proposed approach uses actuators to produce more significant contractions than the required ones. It is possible to provide offsets and use different activation regions to improve the closed-loop bandwidth for the whole movement and not only the contraction (13). Using offsets equal to the required contraction, it was found that the base bandwidth increases linearly by 0.0006 Hz. In the case of the used actuators, the bandwidth improves from 0.051 Hz to 0.15 Hz without requiring any external cooling system and keeping the output force. However, if speed is the main objective, it could use thinner TCP actuators. For instance, if an offset of 1 m is used, the final frequency will be 0.6477 Hz. This frequency improvement could be useful for physical rehabilitation therapy and low frequency ADLs, as the minimum frequency for these activities is 0.5 Hz (26, 35).

Considering that contraction speeds depend on the controller and the applied power, another option to improve the system's speed is using agonist and antagonist fibres that allow the system to actuate in two different directions. Their main disadvantage is that they accumulate heat, preventing the actuators' recovery and making them unable to finish the whole pattern after three cycles (1). The use of long actuators could also benefit this structure. It will be possible to obtain the same displacement as with a smaller actuator but with the advantage of reducing the temperature. It will be harder to saturate the actuators, and it will be possible to go for higher frequencies. Moreover, as noticed from both the isotonic and the closed-loop controllers' experiments, the consumed power is related to the produced stroke rather than the length of the actuator, so in theory, the power consumption will not increase if the activation frequencies are the same. Nevertheless, research on the variable stiffness actuator and stiffness control algorithm is missing to implement a system of this characteristic.

Conclusion

The work in this paper presents the study on the usage of longer TCP actuators to improve the frequency and temperature characteristics of the TCP actuators, where it was found that the strain is independent of the length. However, electrothermal properties change with the length. As a result, the activation temperature to obtain displacement can be reduced with longer actuators. Furthermore, a new strategy to increase TCP actuators' speed without external cooling systems is presented. The model takes into consideration the advantages of long actuator fibres. This was done by estimating an electromechanical system model through an isotonic contraction test. The model was invariant on the length, meaning that the actuators behave similarly independently of the size. Then a PID controller was implemented to control the displacement of the actuator, in the case of the contraction is dependent on the applied power. However, it was found that the cooling time can also be improved by varying the activation section of the used actuator, so having long actuators can improve linear movement by increasing its length. Furthermore, the temperature generated by the TCP fibres is reduced by increasing length.

Data availability

The datasets generated during and/or analysed during the current study are available from the corresponding author upon reasonable request.

Conflict of interest

NA

Acknowledgements

NA

Ethical statement

NA

Funding

NA

References

1. Copaci D, Martín F, Moreno L, Blanco D. SMA based elbow exoskeleton for rehabilitation therapy and patient evaluation. IEEE Access. 2019;7:31473-84.
2. Lerner ZF, Harvey TA, Lawson JL. A Battery-Powered Ankle Exoskeleton Improves Gait Mechanics in a Feasibility Study of Individuals with Cerebral Palsy. Annals of Biomedical Engineering. 2019;47(6):1345-56.
3. Graham HK, Rosenbaum P, Paneth N, Dan B, Lin JP, Damiano DL, et al. Cerebral palsy. Nature Reviews Disease Primers. 2016;2:15082.
4. Patane F, Rossi S, Del Sette F, Taborri J, Cappa P. WAKE-Up Exoskeleton to Assist Children With Cerebral Palsy: Design and Preliminary Evaluation in Level Walking. IEEE Transactions on Neural Systems and Rehabilitation Engineering. 2017;25(7):906-16.
5. Reinkensmeyer DJ. JNER at 15 years: analysis of the state of neuroengineering and rehabilitation. J Neuroeng Rehabil. 2019;16(1):144.
6. Bützer T, Dittli J, Lieber J, van Hedel HJ, Meyer-Heim A, Lambercy O, et al., editors. PEXO-A Pediatric Whole Hand Exoskeleton for Grasping Assistance in Task-Oriented Training. 2019 IEEE 16th International Conference on Rehabilitation Robotics (ICORR); 2019: IEEE.
7. He Y, Eguren D, Luu TP, Contreras-Vidal JL. Risk management and regulations for lower limb medical exoskeletons: a review. Medical Devices: Evidence and Research. 2017;10:89-107.
8. Veale AJ, Xie SQ. Towards compliant and wearable robotic orthoses: A review of current and emerging actuator technologies. Medical Engineering and Physics. 2016;38(4):317-25.
9. Behboodi A, DeSantis C, Lubsen J, Lee S, editors. A Mechanized Pediatric Elbow Joint Powered by a De-Based Artificial Skeletal Muscle. 2020 42nd Annual International Conference of the IEEE Engineering in Medicine & Biology Society (EMBC); 2020: IEEE.
10. Ugurlu B, Forni P, Doppmann C, Sariyildiz E, Morimoto J. Stable Control of Force, Position, and Stiffness for Robot Joints Powered via Pneumatic Muscles. IEEE Transactions on Industrial Informatics. 2019;15(12):6270-9.
11. Haines CS, Lima MD, Li N, Spinks GM, Foroughi J, Madden JD, et al. Artificial muscles from fishing line and sewing thread. science. 2014;343(6173):868-72.
12. Wu L, Chauhan I, Tadesse Y. A Novel Soft Actuator for the Musculoskeletal System. Advanced Materials Technologies. 2018;3(5).
13. Tang X, Li K, Liu Y, Zhou D, Zhao J. A soft crawling robot driven by single twisted and coiled actuator. Sensors and Actuators A: Physical. 2019;291:80-6.
14. Zhang J, Sheng J, ONeill CT, Walsh CJ, Wood RJ, Ryu JH, et al. Robotic Artificial Muscles: Current Progress and Future Perspectives. IEEE Transactions on Robotics. 2019.
15. Hyeon K, Jeong J, Chung C, Cho M, Hussain S, Kyung K-U. Design of a Wearable Mechanism with Shape Memory Alloy (SMA)-based Artificial Muscle for Assisting with Shoulder Abduction. IEEE Robotics and Automation Letters. 2022;7(4):10635-42.

16. Saharan L, de Andrade MJ, Saleem W, Baughman RH, Tadesse Y. iGrab: hand orthosis powered by twisted and coiled polymer muscles. Smart Materials and Structures. 2017;26(10):105048.
17. Cenciarini M, Dollar AM, editors. Biomechanical considerations in the design of lower limb exoskeletons. 2011 IEEE International conference on rehabilitation robotics; 2011: IEEE.
18. Gonzalez-Vazquez A, Garcia L, Kilby J, McNair P. Soft Wearable Rehabilitation Robots with Artificial Muscles based on Smart Materials: A Review. Advanced Intelligent Systems. 2023:2200159.
19. Hiraoka M, Nakamura K, Arase H, Asai K, Kaneko Y, John SW, et al. Power-efficient low-temperature woven coiled fibre actuator for wearable applications. Sci Rep. 2016;6:36358.
20. Haines CS, Niemeyer G, editors. Closed-loop temperature control of nylon artificial muscles. 2018 IEEE/RSJ International Conference on Intelligent Robots and Systems (IROS); 2018: IEEE.
21. Yip MC, Niemeyer G. On the Control and Properties of Supercoiled Polymer Artificial Muscles. IEEE Transactions on Robotics. 2017;33(3):689-99.
22. Edmonds BP, Trejos AL, editors. Frequency Response Analysis of Actively Cooled Nylon Twisted Coiled Actuators for Use in Wrist Rehabilitation Devices. 2020 8th IEEE RAS/EMBS International Conference for Biomedical Robotics and Biomechatronics (BioRob); 2020: IEEE.
23. Chossat JB, Chen DKY, Park YL, Shull PB. Soft Wearable Skin-Stretch Device for Haptic Feedback using Twisted and Coiled Polymer Actuators. IEEE Trans Haptics. 2019.
24. Saharan L, Tadesse Y, editors. Fabrication parameters and performance relationship of twisted and coiled polymer muscles. ASME 2016 International Mechanical Engineering Congress and Exposition; 2016: American Society of Mechanical Engineers Digital Collection.
25. Edmonds BP, DeGroot CT, Trejos AL. Thermal modeling and characterization of twisted coiled actuators for upper limb wearable devices. IEEE/ASME Transactions on Mechatronics. 2020;26(2):966-77.
26. Murphy V, Edmonds BP, Trejos AL. Characterisation and Control of a Woven Biomimetic Actuator for Wearable Neurorehabilitative Devices. Actuators. 2021;10(2):37.
27. Patiño AG, Ferrone A, Gastélum CGD, Menon C, editors. A novel biomedical technology based on the use of artificial muscles to assist with hand functions. 2018 IEEE 9th Annual Information Technology, Electronics and Mobile Communication Conference (IEMCON); 2018: IEEE.
28. Cho KH, Song M-G, Jung H, Yang SY, Moon H, Koo JC, et al., editors. Fabrication and modeling of temperature-controllable artificial muscle actuator. 2016 6th IEEE International Conference on Biomedical Robotics and Biomechatronics (BioRob); 2016: IEEE.
29. Tang X, Li K, Chen W, Zhou D, Liu S, Zhao J, et al. Temperature self-sensing and closed-loop position control of twisted and coiled actuator. Sensors and Actuators A: Physical. 2019;285:319-28.
30. Proto A, Penhaker M, Bibbo D, Vala D, Conforto S, Schmid M. Measurements of generated energy/electrical quantities from locomotion activities using piezoelectric wearable sensors for body motion energy harvesting. Sensors. 2016;16(4):524.
31. Mann KA, Wernere FW, Palmer AK. Frequency spectrum analysis of wrist motion for activities of daily living. Journal of Orthopaedic research. 1989;7(2):304-6.
32. Vicario R, Calanca A, Dimo E, Murr N, Meneghetti M, Ferro R, et al., editors. Benchmarking Force Control Algorithms. The 14th PErvasive Technologies Related to Assistive Environments Conference; 2021; Corfu, Greece.
33. Pittaccio S, Viscuso S, Rossini M, Magoni L, Pirovano S, Villa E, et al. SHADE: A Shape-Memory-Activated Device Promoting Ankle Dorsiflexion. Journal of Materials Engineering and Performance. 2009;18(5-6):824-30.
34. Hope J, McDaid A. Development of wearable wrist and forearm exoskeleton with shape memory alloy actuators. Journal of Intelligent & Robotic Systems. 2017;86(3-4):397.
35. Jeong J, Hyeon K, Han J, Park CH, Ahn S-Y, Bok S-K, et al. Wrist Assisting Soft Wearable Robot with Stretchable Coolant Vessel integrated SMA Muscle. IEEE/ASME Transactions on Mechatronics. 2021;27(2):1046-58.